Asian Journal of Chemistry; Vol. 37, No. 8 (2025), 2037-2041

ASIAN JOURNAL OF CHEMISTRY

https://doi.org/10.14233/ajchem.2025.34076

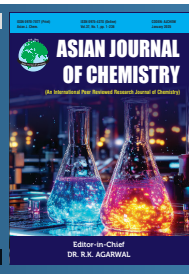

Green Synthesis of Zinc Oxide Nanoparticles using *Hibiscus rosa-sinensis* Leaves Extract: Structural, Morphological, Bioactivity and Photocatalytic Properties

S. Aron Rabi[1,*] and A. Joseph Sagaya Kennedy[2]

[1]PG & Research Department of Physics, St. Xavier's College (Autonomous), (Affiliated to Manonmaniam Sundaranar University) Palayamkottai, Tirunelveli-627002, India
[2]Department of Physics, SRM TRP Engineering College, (Affiliated to Anna University), Tiruchirappalli-621105, India

*Corresponding author: E-mail: aron.rb@gmail.com

Received: 17 May 2025; *Accepted*: 24 July 2025; *Published online*: 31 July 2025; AJC-22083

Zinc oxide nanoparticles (ZnO NPs) were synthesized using an eco-friendly green synthesis approach, with *Hibiscus rosa-sinensis* leaf extract serving as both a stabilizing and capping agent. The bioactive compounds present in the leaf extract facilitated the formation of ZnO nanoparticles by stabilizing the zinc salt precursor during the synthesis process. The resulting ZnO nanoparticles were coated with biomolecules from the *H. rosa-sinensis* extract, enhanced the biological activity. Comprehensive characterization of the synthesized ZnO nanoparticles was performed using a range of advanced techniques, including X-ray diffraction (XRD) to determine crystalline structure, Fourier transform infrared spectroscopy (FT-IR) to identify functional groups, UV-Vis spectroscopy to analyze the optical properties and electron microscopy (SEM and TEM) to examine their surface morphology and particle size. An 81.3% breakdown of acid black 1 (AB 1) dye was observed in sunlight, with the degradation rate escalating as the irradiation duration increased. The antimicrobial activity against *Staphylococcus aureus* and *Bacillus subtilis* show higher results compared to *Escherichia coli* and *Salmonella typhimurium*.

Keywords: Green synthesis, *Hibiscus rosa-sinensis*, Zinc oxide, Acid black 1 dye, Antimicrobial activity, Degradation.

INTRODUCTION

Zinc oxide nanoparticles for inorganic compounds with a wide range of applications due to their properties. Zinc oxide has a bandgap energy of around 3.37 eV, it is useful in electronic devices like LEDs and solar cells. Zinc oxide is also used in sunscreens, cosmetics and textiles for its UV-blocking properties [1-5]. ZnO nanoparticles have antimicrobial properties and are used in antibacterial coatings, textiles and medical devices [6,7]. It exhibits piezoelectric properties and is used in sensors, resonators and actuators [8-10]. ZnO nanoparticles can be synthesized through chemical vapour deposition, sol-gel synthesis, hydrothermal methods and green synthesis using plant extracts or other eco-friendly approaches [11-13].

Plant extracts have recently been used to generate ZnO NPs successfully [14-16]. This approach is an eco-friendly and sustainable production process [17,18]. Importantly, no additional chemical reagents were involved in the process, highlighting its eco-friendly nature. In nanoparticle synthesis, certain phytochemicals are essential for reducing metal ions and stabilizing the resulting nanoparticles. Plant extracts from different species provide a diverse array of phyto-chemicals with strong reduction potential, making them a valuable system for the nanoparticle synthesis [19,20].

This study focused on synthesizing zinc oxide (ZnO) nanoparticles using *Hibiscus rosa-sinensis* leaf extracts as a natural stabilizing and capping agent. The plant-based capping agent coats the ZnO nanoparticles, helping to maintain their small size. The synthesis process is entirely free of additional chemical reagents, as the compounds in the plant extract create the necessary alkaline conditions and prevent excessive nanoparticle growth.

EXPERIMENTAL

Zinc nitrate hexahydrate, sodium hydroxide and the solvents used in this work were purchased from Merck Chemical Reagent Co. Ltd., India. Acid black 1 (AB 1) dye was procured from

Sigma-Aldrich, USA. The infrared (IR) spectrum was recorded using an Avatar-330 FT-IR spectrophotometer. The powder X-ray diffraction (XRD) pattern of ZnO was captured with an X'Per PRO diffractometer, equipped with Cu*K*α radiation (λ = 1.5406 Å) and operating at 2.2 kW. The peak positions were compared against the standard reference files to determine the crystalline phase. Scanning electron microscopy (SEM) images were obtained from gold-coated samples using a JEOL-JSM 5610 LV. Diffuse reflectance spectra were measured with a Shimadzu UV-2450 instrument. Transmission electron microscopy (TEM) was conducted on a Hitachi H-7000, Japan, at an acceleration voltage of 100 kV. Absorption spectra were collected using an OCEAN OPTICS USB 4000 UV spectrometer.

Preparation of plant leaf extract: *Hibiscus rosa sinensis* plant leaves were collected in Tirunelveli district (8.8550º N, 77.6522º E), India and authenticated by the botanist of the institution. The leaves were cleaned with distilled water to remove dust and other contaminants. The leaves were dried at room temperature (30 ºC) and then chopped and ground finely. Dried leave powder (1 g) was boiled for 30 min in 100 mL of distilled water until the colour changed. The mixture was cooled, filtered and centrifuged to collect the leaf extract from the supernatant solution.

Synthesis of ZnO nanoparticles: The ZnO nanoparticles were prepared using a reported procedure with slight modification [21]. About 30 mL of aqueous *H. rosa-sinensis* extract was added to 100 mL of distilled water. Separately, 100 mL of 0.5 M zinc nitrate solution was prepared in distilled water and the leaf extract was slowly introduced into this solution while stirring. After 30 min, the mixture turned light yellow and then NaOH was added to adjust the pH and the solution was stirred at 60 ºC for 1 h until a precipitate formed. The precipitate was filtered and dried in a hot air oven at 70 ºC for 3 h. The dried product was ground into a fine powder and then heated in a furnace at 400 ºC for 1 h.

Photodegradation experiments: The photocatalytic performance of the synthesized ZnO nanoparticles was assessed by degrading AB 1 azo dye under visible light using an immersion type photoreactor (make: Heber immersion photoreactor HP-SLJV16254). This setup featured a double-walled quartz reactor with a capacity of 175 mL. A narrow inlet tube facilitated the passage of coolant from the bottom to the outlet through the annular space. In the center of the cylindrical reactor, a light source (either UV or visible) was positioned inside the quartz tube. For the current experiment, a 150 W tungsten visible lamp was employed and the experimental solution's temperature was maintained at 25 ºC by circulating water during the process. The entire setup was placed on a magnetic stirrer to ensure thorough mixing of the catalyst. For each trial, a suspension containing 20 mg of photocatalyst in 100 mL of 10 ppm AB 1 dye solution was stirred in the dark for 30 min to establish the adsorption/desorption equilibrium between the photocatalyst and the dye. Following this, the suspension was exposed to visible light, with 4 mL aliquots taken at specific intervals and centrifuged to separate the photocatalyst particles. The supernatant was analyzed by measuring changes in absorbance at 320 nm in the UV-visible spectrum of AB 1 dye.

RESULTS AND DISCUSSION

XRD analysis: X-ray diffraction was used to characterize the phase purity and crystalline size of ZnO nanoparticles by the green synthesis method. The XRD pattern of zinc oxide nanoparticles is shown in Fig. 1. The characteristic diffraction peaks (2θ) for ZnO nanoparticles obtained are 31.67º, 34.28º, 36.18º, 47.44º, 56.46º, 62.76º, 68.92º, corresponding to the *hkl* peaks of ZnO nanoparticles (100), (002), (101), (102), (110), (103), (201) planes [22-24]. The crystal system of the ZnO nanoparticle is a hexagonal wurtzite crystal structure. The obtained values were well coincidental with the JCPDS file No. 01-089-0510. The sharp peaks show that the ZnO nanoparticles are

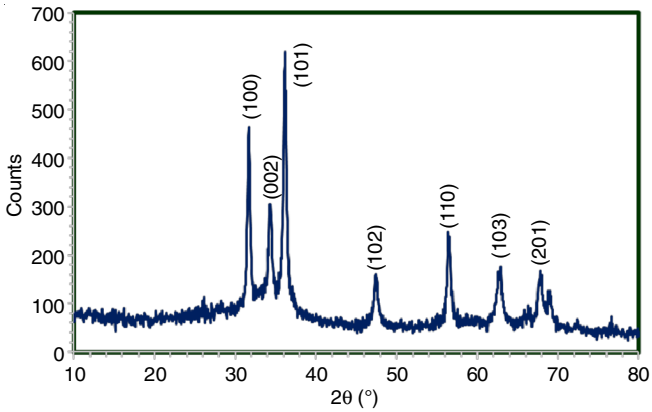

Fig. 1. XRD pattern of synthesized ZnO NPs from *H. rosa-sinensis* leaves extract

crystalline in nature and the crystalline size of the ZnO nanoparticles can be determined using Debye-Scherrer equation (eqn. 1):

$$D = \frac{K\lambda}{\beta\cos\theta} \quad (1)$$

where D is the size of the particle; K is the Scherrer's constant (K = 0.94); λ is the X-ray wavelength (1.54178 Å) and β is the full-width at half maximum of the diffraction peak. The dislocation density measures the number of dislocations present in a unit volume of a crystalline material. The dislocation density was calculated using the following formula (eqn. 2):

$$\delta = \frac{1}{D^2} \quad (2)$$

The root mean square of the variations in the lattice parameters across the individual crystallites, usually across microscopic distances. The microstrain value can be calculated using eqn. 3:

$$\Sigma = \frac{\beta}{4\tan\theta} \quad (3)$$

Specific surface area (SSA) describes the properties of the material and determines its type and structure. The specific surface area is directly proportional to the surface-to-volume ratio of nanoparticles. The SSA value was calculated using eqn. 4:

$$\text{Specific surface area (SSA)} = \frac{6\times10^3}{D\times\rho} \quad (4)$$

Thus, the average crystallite size, microstrain and dislocation density of the green synthesized ZnO nanoparticles are calculated and the values are given in Table-1.

UV-visible spectral analysis: Fig. 2a shows the UV-Vis absorption spectrum of green synthesized ZnO nanoparticles. Strong absorption bands of the biosynthesized material were observed in the range of 337 nm to the entire visible region. The absence of additional absorbance peak confirms that the synthesized products are pure ZnO nanoparticles. Tauc plot bandgap of ZnO nanoparticles was also observed. The prepared ZnO nanoparticles show a very sharp band gap value of 3.16 eV (Fig. 2b). The smaller band gap will easily categorize a photocatalytic reaction of the nanoparticles and show the good photocatalytic activity.

Fourier transform infrared spectroscopy (FT-IR): FT-IR spectrum of the prepared ZnO sample was recognized in the wavelength range of 4000-400 cm^{-1} (Fig. 3). The FT-IR spectra exhibited a broad peak at around 3433 cm^{-1} is due to the O-H stretching of alcoholic and phenolic groups. Peaks around 3433 and 1642 cm^{-1} suggest the presence of O–H and possibly C=O groups, which may come from water molecules or organic functional groups in the leaf extract. The peak at 2923 cm^{-1} confirmed the C–H vibrations of the organic funtional groups. The peak at 2426 cm^{-1} could correspond to the CO stretching vibrations, whereas the peak at 1642 cm^{-1} usually indicates the C=O stretching vibrations, confirmed the presence of carbonyl groups. It can be related to organic compounds such as ketones, aldehydes or amides present in the leaf extract or to absorbed water (H–O–H bending vibrations). The peaks at 1384 cm^{-1} peak suggests the C–N stretching or nitrate groups, while at 1038 cm^{-1} indicates C–O vibrations, likely from the organic molecules in the leaf extract. The peak in the region between 600 and 400 cm^{-1} is assigned to Zn-O stretching vibration confirming ZnO nanoparticles synthesized using *H. rosa sinensis* extract as a reducing and capping agent. These peaks highlight both the ZnO nanoparticles formation and the presence of organic functional groups from the leaf extract, which often play a role as capping or stabilizing agents during the green synthesis of ZnO nanoparticles [25].

Morphological analysis: The surface morphologies of biosynthesized ZnO nanoparticles were studied by using SEM and TEM and the results are presented in Fig. 4. Fig. 4a-b depict the SEM images of the green-synthesized ZnO nanoparticles, confirming their spherical morphology, which appears aggregated due to the presence of a capping agent that stabilizes the nanoparticles. The morphology of biosynthesized ZnO nanoparticles was further confirmed by its TEM images (Fig. 4c-d), the spherical-shaped particles are agglomerated in which the presence of plant extract, contains flake-type shapes in aggregated form. This aggregation/agglomeration may be caused by to polarity and electrostatic attraction of ZnO nanoparticles.

TABLE-1
PARAMETERS DERIVED FROM XRD OF ZnO NANOPARTICLES

Observed 2θ	*hkl*	Crystalline size (nm) (D)	Dislocation density × 10^{14} lines/m^2 (δ)	Micro strain (ε) ×10^{-6}	Specific surface area ($m^2/g \times 10^3$)
31.6799	100	26.236	1.4527	4.843	4.0765
34.2877	002	52.845	3.5808	2.2204	2.0238
36.1860	101	21.244	2.2157	5.2565	5.0343
47.4400	102	27.569	1.3156	3.1271	3.8793
56.4693	110	45.419	4.8475	1.5991	2.3547
62.7616	103	19.712	2.5735	3.3787	5.4256
68.9257	201	24.492	1.667	2.5023	4.3667
Average values	–	31.074	2.52182	3.2753	3.88012

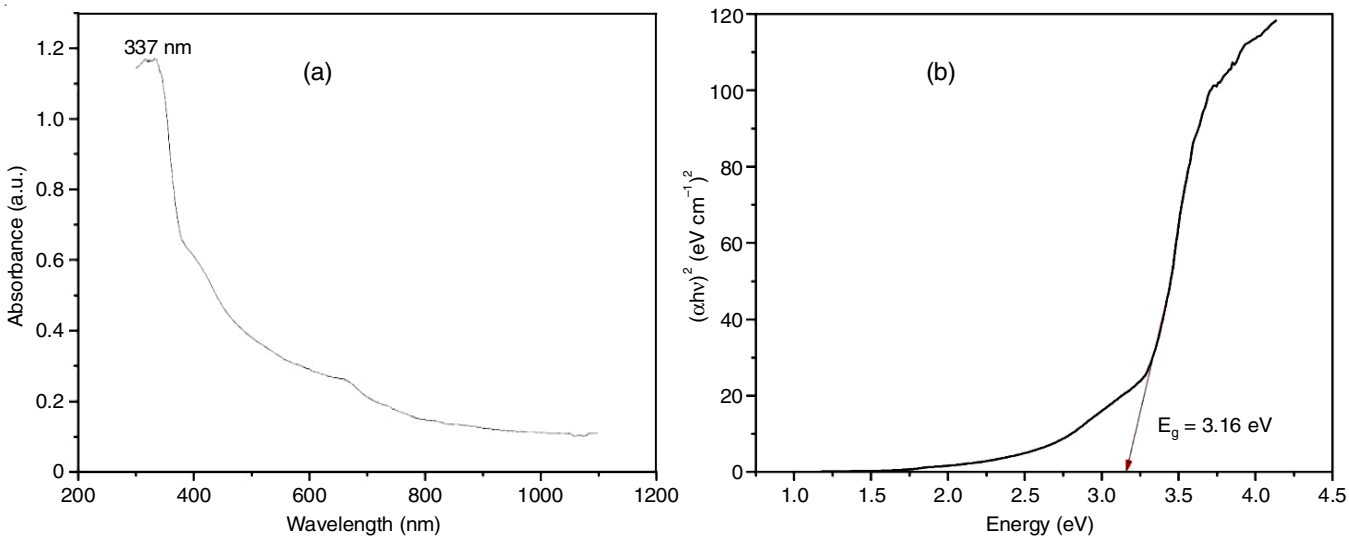

Fig. 2. (a) UV-Visible absorption spectrum and (b) bandgap energy of synthesized ZnO NPs from *H. rosa-sinensis* leaves extract

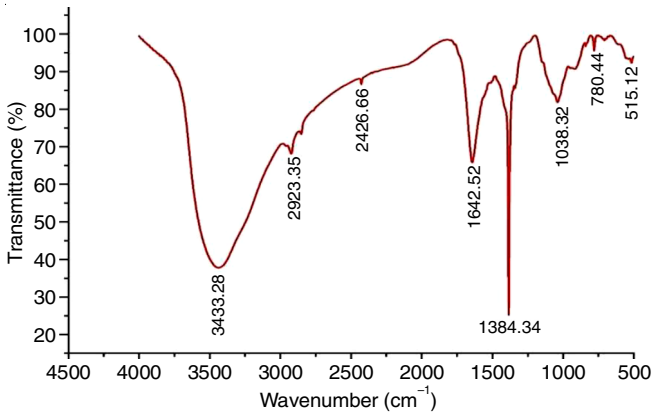

Fig. 3. FT-IR spectrum of synthesized ZnO NPs from *H. rosa-sinensis* leaves extract

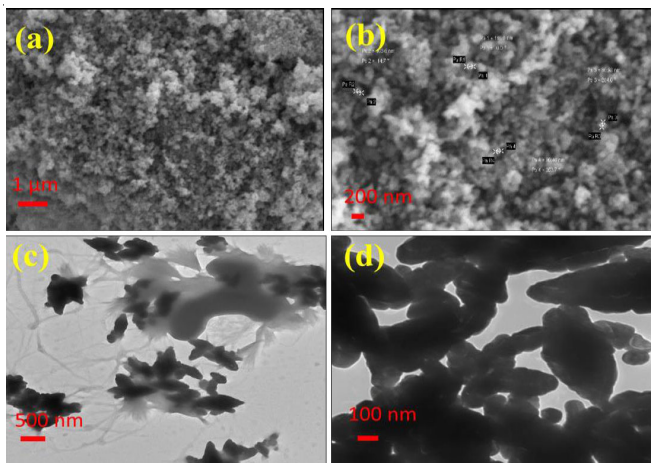

Fig. 4. (a&b) SEM and TEM (c&d) images of synthesized ZnO NPs from *H. rosa-sinensis* leaves extract

Antimicrobial activity: The antibacterial activity of biogenic ZnO nanoparticles was investigated against selected four pathogens (Gram-positive and Gram-negative) such as *Staphylococcus aureus*, *Bacillus subtilis*, *Escherichia coli* and *Salmonella typhimurium* by using the disc diffusion method [26] and the results are shown in Table-2. The biosynthesized ZnO nanoparticles using *H. rosa sinensis* leaf extract exhibited strong antimicrobial activity. The different amount of ZnO (50 and 100 µg) is taken for the process and dispersed in a DMSO solution. Then control (streptomycin) was placed at the center and samples at the edges. *Staphylococcus aureus* and *Bacillus subtilis* show higher results compared to *Escherichia coli* and *Salmonella typhimurium*. Antimicrobial activity of ZnO nanoparticles attached to the bacterial cell membrane, which may disrupt the membrane plasma structure and damage the bacterial cell integrity, resulting in the leakage of intracellular contents and leading to the cell death.

Photocatalytic activity: The photocatalytic performance of the biosynthesized ZnO NPs was tested under visible light for the degradation of AB 1 dye, with the results shown in Fig. 5a-b. AB 1 is resistant to self-photolysis and remains stable when exposed to the visible light. In the absence of light, ZnO nanoparticles adsorbed approximately 12% of dye onto its surface. However, when exposed to visible light, ZnO NPs achieved about 81.3% degradation, with the degradation rate increasing as the irradiation time extended. The UV-Vis spectra of AB 1 dye at various irradiation times with ZnO nanoparticles (Fig. 5b) indicate that the dye undergoes complete breakdown over time and the intermediates do not absorb at the analytical wavelength.

Mechanism: The process of photocatalysis is elucidated by the mechanism whereby the semiconductor materials, when subjected to light of a certain wavelength and intensity, result in the excitation of electrons (e^-) within the valence band (VB). These excited electrons are then transferred to the conduction band (CB) [22,27,28]. The excited electrons react with dissolved oxygen to form superoxide radical anions, while the holes (h^+)

TABLE-2
ANTIMICROBIAL ACTIVITY OF BIO-SYNTHESIZED ZnO NANOPARTICLES

Pathogens	*Staphylococcus aureus* (mm)	*Bacillus subtilis* (mm)	*Escherichia coli* (mm)	*Salmonella typhimurium* (mm)
50 µg	13	11	12	10
100 µg	14	12	8	10
Control	16	17	19	20

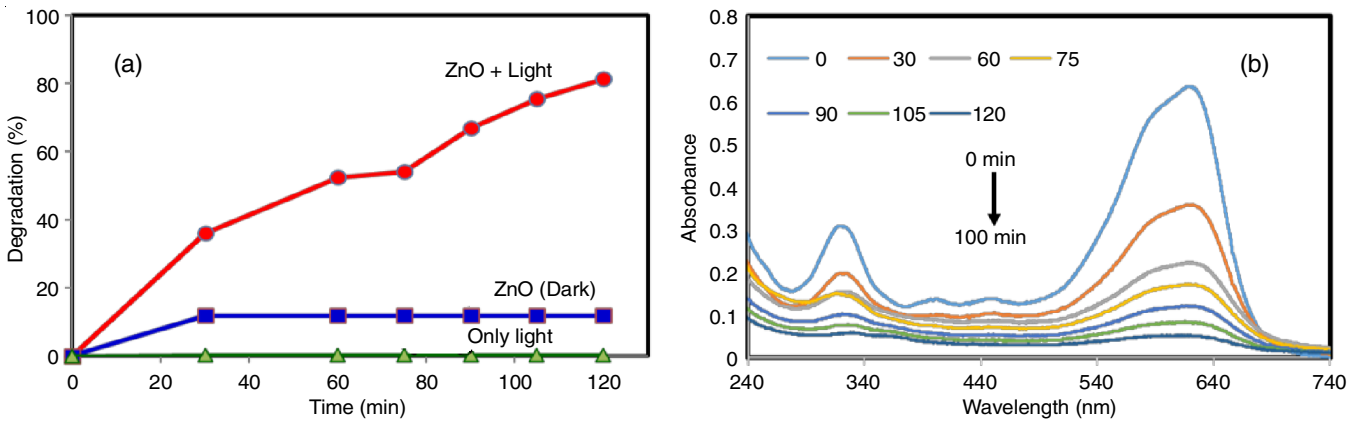

Fig. 5. (a) Photocatalytic degradation AB 1 dye, (b) UV-Vis spectra of AB 1 ye with different times of irradiation with biogenic ZnO NPs

left behind in the VB are used to oxidize water molecules, generate hydroxyl radicals or directly oxidize AB 1 dye. As a result, various sub-processes, such as charge excitation, transfer, recombination, separation and subsequent photochemical reactions on the semiconductor surface, occur during the process (Fig. 6). Based on the aforementioned discussion, the photocatalytic degradation of AB 1 molecules can be summarized as: initially e^-–h^+, separation happened when the ZnO NPs surface was irradiated with light (eqn. 5) and then AB 1 molecules were oxidized by the produced superoxide ($O_2^{\bullet-}$) radical anions and finally converted to H_2O, CO_2 and other mineralization byproducts.

$$ZnO + h\nu \rightarrow ZnO\ (e^-\ (CB) + h^+\ (VB)) \quad (5)$$

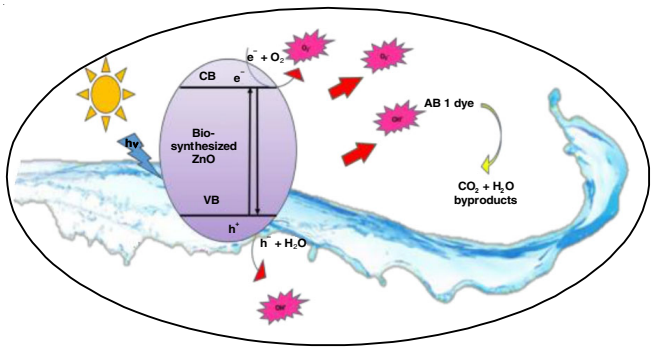

Fig. 6. Mechanism of degradation of acid black 1 (AB 1) dye with ZnO NPs

Conclusion

Zinc oxide nanoparticles were effectively synthesized utilizing an eco-friendly synthesis approach with the extract from *Hibiscus rosa sinensis* leaves. The XRD results confirms the structure of ZnO nanoparticles and the formation of a narrow peak with a Bragg's angle of 2θ suggests the crystalline nature and wurtzite structure. Stabilization of the ZnO NPs occurs with some capping agents, which are confirmed by the sharp peaks. The intense Bragg's angle reflection suggests the strong X-ray scattering centers in the crystalline phase, which is due to the capping agents. Based on the UV-Vis spectroscopy, the ZnO nanoparticles have distinguished colours in colloidal solutions due to their miniature dimension. The SEM and TEM analyses confirm the formation of ZnO nanoparticles of spherical size with aggregation. The biosynthesized ZnO nanoparticles have proved effective antimicrobial agents against *S. aureus, B. subtilis, E. coli* and *S. typhimurium* bacteria. Moreover, ZnO nanoparticles effectively degraded the acid black 1 dye under visible light.

CONFLICT OF INTEREST

The authors declare that there is no conflict of interests regarding the publication of this article.

REFERENCES

1. B. Krishnakumar and M. Swaminathan, *Spectrochim. Acta A Mol. Biomol. Spectrosc.*, **81**, 739 (2011); https://doi.org/10.1016/j.saa.2011.07.019
2. J. Zeng, H.W. Yang, Y.F. Tong, G.Y. Dong, D.X. Liu, C. Wen, Y. Ren, M. Chen, X.Y. Li, Z. Xu, Y. We and Q.Y. Dai, *Opt. Mater.*, **154**, 115766 (2024); https://doi.org/10.1016/j.optmat.2024.115766
3. S. Ranjitha, S. Bhuvaneswari, C. Sudhakar and V. Aroulmoji, *Chem. Phys. Impact*, **9**, 100735 (2024); https://doi.org/10.1016/j.chphi.2024.100735
4. J.Y. Kim, P. Vincent, J. Jang, M.S. Jang, M. Choi, J.H. Bae, C. Lee and H. Kim, *J. Alloys Compd.*, **813**, 152202 (2020); https://doi.org/10.1016/j.jallcom.2019.152202
5. M. Kamruzzaman, *Nanoscale Adv.*, **2**, 286 (2020); https://doi.org/10.1039/C9NA00523D
6. A. Giedraitiene, M. Ru•auskas, R. Šiug•diniene, S. Tuckute, K. Grigonis and D. Milcius, *Nanomaterials*, **14**, 1264 (2024); https://doi.org/10.3390/nano14151264
7. P. Monika, R.H. Krishna, Z. Hussain, K. Nandhini, S.J. Pandurangi, T. Malek and S. Girish Kumar, *Biomater. Adv.*, **172**, 214246 (2025); https://doi.org/10.1016/j.bioadv.2025.214246
8. R.K. Pandey, J. Dutta, S. Brahma, B. Rao and C.-P. Liu, *J. Phys. Mater.*, 4, 044011 (2021); https://doi.org/10.1088/2515-7639/ac130a
9. N. Bhadwal, R.B. Mrad and K. Behdinan, *Sensors*, **23**, 3859 (2023); https://doi.org/10.3390/s23083859
10. A.L. Nikolaev, M.A. Kazmina, N.V. Lyanguzov, K.G. Abdulvakhidov, and E.M. Kaidashev, *J. Adv. Dielectr.*, **12**, 2160020 (2022); https://doi.org/10.1142/S2010135X21600201
11. M. Bandeira, M. Giovanela, M. Roesch-Ely, D.M. Devine and J. da Silva Crespo, *Sustain. Chem. Pharm.*, **15**, 100223 (2020); https://doi.org/10.1016/j.scp.2020.100223
12. S. Zeghoud, H. Hemmami, B.B. Seghir, I.B. Amor, I. Kouadri, A. Rebiai, M. Messaoudi, S. Ahmed, P. Pohl and J. Simal-Gandara, *Mater. Today Commun.*, **33**, 104747 (2022); https://doi.org/10.1016/j.mtcomm.2022.104747
13. F.T.Z. Toma, M.S. Rahman and K.H. Maria, *Discov. Mater.*, **5**, 60 (2025); https://doi.org/10.1007/s43939-025-00201-1
14. N. Rani, P. Singh, S. Kumar, P. Kumar, V. Bhankar and K. Kumar, *Mater. Res. Bull.*, **163**, 112233 (2023); https://doi.org/10.1016/j.materresbull.2023.112233
15. C. Hano and B.H. Abbasi, *Biomolecules*, **12**, 31 (2022); https://doi.org/10.3390/biom12010031
16. H. Singh, N.F. Desimone, S. Pandya, S. Jasani, N. George, M. Adnan, A. Aldarhami, A.S. Bazaid and S.A. Alderhami, *Int. J. Nanomedicine*, **18**, 4727 (2023); https://doi.org/10.2147/IJN.S419369
17. H.Y. Chai, S.M. Lam and J.C. Sin, *AIP Conf. Proc.*, **2157**, 020042 (2019); https://doi.org/10.1063/1.5126577
18. B. Krishnakumar, A. Alsalme, F.A. Alharthi, D. Mani, K. Anandan, P. Amutha and A.J.F.N. Sobral, *Opt. Mater.*, **113**, 110854 (2021); https://doi.org/10.1016/j.optmat.2021.110854
19. A. Hosseingholian, *J. Mol. Struct.*, **1279**, 134 (2023); https://doi.org/10.1016/j.mtsust.2023.100500
20. S.J.P. Begum, S. Pratibha, J.M. Rawat, D. Venugopal, P. Sahu, K.A. Qureshi and M. Jaremko, *Pharmaceuticals*, **15**, 455 (2022); https://doi.org/10.3390/ph15040455
21. S. Lenka and S.K. Badamali, *J. Mol. Catal.*, **536**, 112918 (2023); https://doi.org/10.1016/j.mcat.2023.112918
22. I.S. Saputra, E. Nurfani, A.G. Fahmi, A.H. Saputro, D.O.B. Apriandanu, D. Annas and Y. Yulizar, *Vacuum*, **227**, 113434 (2024); https://doi.org/10.1016/j.vacuum.2024.113434
23. I.H. Alsohaimi, N.F. Alotaibi, A.M. Albarkani, Q. Chen, S.M.N. Moustafa, M.S. Alshammari and A.M. Nassar, *Alex. Eng. J.*, **83**, 113 (2023); https://doi.org/10.1016/j.aej.2023.10.037
24. N. Yousefi, Y. Zahedi, A. Yousefi, G. Hosseinzadeh and M. Jekle, *Int. J. Biol. Macromol.*, **265**, 130849 (2024); https://doi.org/10.1016/j.ijbiomac.2024.130849
25. A. Vijayakumar, R. Mohan and P. Jayaprakash, *J. Indian Chem. Soc.*, **101**, 101375 (2024); https://doi.org/10.1016/j.jics.2024.101375
26. R.A. Alghamdi, M.H. Al-Zahrani, M.H. Al-Zahrani, L.R. Altarjami, W. Al Abdulmonem, N. Samir, A. Said, A.A. Shami, W.S. Mohamed and M. Ezzeldien, *Front. Bioeng. Biotechnol.*, **11**, 1283898 (2023); https://doi.org/10.3389/fbioe.2023.1283898
27. K. Balu, S. Kaliyamoorthy, M. Durai, A. Aguiar, M.C.M. Sobral, I. Muthuvel, S. Kumaravel, B. Avula, A.J.F.N. Sobral and Y.H. Ahn, *Inorg. Chem. Commun.*, **154**, 110973 (2023); https://doi.org/10.1016/j.inoche.2023.110973.
28. M.-R. Zamani-Meymian, N. Naderi and M. Zareshahi, *Ceram. Int.*, **48**, 34948 (2022); https://doi.org/10.1016/j.ceramint.2022.08.084